

# Simulation of the Development and Interaction of Instabilities in a Relativistic Electron Beam under Variation of the Beam Wall Thickness

A. A. Badarin<sup>a, b</sup>, S. A. Kurkin<sup>a, b</sup>, A. A. Koronovskii<sup>b</sup>, A. O. Rak<sup>c</sup>, and A. E. Hramov<sup>a, b\*</sup>

<sup>a</sup> Saratov State University, Saratov, 410012 Russia

<sup>b</sup> Yuri Gagarin State Technical University, Saratov, 410054 Russia

<sup>c</sup> Belorussian State University of Informatics and Radioelectronics, Minsk, 220013 Belarus

\*e-mail: hramovae@gmail.com

Received February 25, 2016; in final form, May 6, 2016

**Abstract**—The development and interaction of Bursian and diocotron instabilities in an annular relativistic electron beam propagating in a cylindrical drift chamber are investigated analytically and numerically as functions of the beam wall thickness and the magnitude of the external uniform magnetic field. It is found that the interaction of instabilities results in the formation of a virtual cathode with a complicated rotating helical structure and several reflection regions (electron bunches) in the azimuthal direction. It is shown that the number of electron bunches in the azimuthal direction increases with decreasing beam wall thickness and depends in a complicated manner on the magnitude of the external magnetic field.

DOI: 10.1134/S1063780X17030047

## 1. INTRODUCTION

Relativistic electron beams (REBs) are of considerable interest for modern high-power electronics. Active studies of the processes of REB transport and different types of REB instabilities are motivated, first of all, by the wide scope of REB applications. Intense charged particle beams are used in many modern oscillators and amplifiers of microwave and terahertz ranges [1–5], such as gyrotrons, vircators, relativistic traveling wave tubes, backward wave tubes, magnetrons, and free-electron lasers. Propagating in the drift space, REBs often demonstrate complicated space charge dynamics, resulting in the formation of electron structures [6–11]. Under certain conditions, various types of instabilities (diocotron, slipping, Pierce, Bursian, and others) can develop in the REB [12–18].

Bursian instability develops when an electron beam with a current density exceeding a certain critical value propagates in the vacuum drift chamber. This instability imposes restrictions on the maximum current that can be transported through the equipotential drift space [19–23] and also leads to the appearance of a nonstationary virtual cathode (VC), the intense oscillations of which are utilized in a whole class of high-power microwave devices—VC-based oscillators and amplifiers (vircators) [1, 24–33]. Bursian instability is caused by a local decrease in the beam potential under the action of the beam space charge. In the course of diocotron instability, the nonuniformity of the current

density (or velocity) in an annular electron beam leads to the appearance of electrical fields and electron drift, which, in turn, results in the amplification of the nonuniformity and fragmentation of the beam into current filaments [34–39]. In particular, diocotron instability can lead to the appearance of vortex and helical structures in the beam, which can negatively affect the operation of a high-power electrovacuum or beam-plasma device.

Many theoretical and experimental works [17, 40–45] were concerned with the physical processes occurring in an REB during the development of instabilities. Nevertheless, the problem of the interaction and coexistence of different instabilities that can simultaneously develop in the REB under certain conditions still remains poorly studied. Therefore, this work is devoted to the study of interaction between Bursian and diocotron instabilities in an annular REB. Special attention is paid to the effect of the beam wall thickness on the dynamics of the system. We note that, in addition to their fundamental importance, such studies are obviously of practical importance, because information on the processes occurring in the REB during these instabilities can be used to develop new types of high-power microwave and terahertz oscillators and amplifiers, as well as to optimize the existing ones.

## 2. MODEL

To numerically study the nonstationary processes of electron–wave interaction in a beam–plasma system, we used the CST Particle Studio software intended for 3D electromagnetic simulations by the method of large particles, which was previously successfully employed in solving various problems of microwave electronics and plasma physics [46]. In the CST Particle Studio package, the excited electromagnetic fields are calculated by solving 3D Maxwell’s equations. The CST Particle Studio allows one to perform reliable numerical simulations of electronic devices with a high accuracy [32, 45, 47–52]. Due to the advanced methods employed in this package, it can be regarded as an efficient and universal instrument supplementing experimental research.

To study the processes occurring in a relativistic vircator, we used the following model (Fig. 1). The system consists of perfectly conducting cylindrical drift chamber  $I$  of length  $L$  and radius  $R$  with an emitter on the left side and coaxial waveguide port  $3$  on the right side. Axisymmetric monovelocity annular REB  $4$  with the current  $I$ , initial electron energy  $W_e$  (in this work, it was set at 850 keV), outer radius  $R_b$ , and wall thickness  $d$  is injected into the system. The beam electrons escape from the drift space onto collector  $5$  and the side walls of the waveguide. In this work, the simulations were performed for the following geometrical parameters of the system:  $L = 45$  mm,  $R = 10$  mm, and  $R_b = 5$  mm. The resonance properties of the electrodynamic system are weakly pronounced, because the system dimensions are much larger than the wavelength of the mode at the fundamental frequency of the vircator. The external uniform magnetic field  $B_0$  is applied along the waveguide axis. It is assumed that the REB injected into the system is formed using a magnetically insulated diode [53]. The total duration of the flat-top current pulse with the amplitude  $I_0$  and a rise time of  $\tau = 1$  ns is  $T = 100$  ns. In these simulations, we have studied the spatiotemporal structures formed in the REB and the distributions of the space charge and current density as functions of the beam wall thickness  $d$  and the external magnetic field  $B_0$ .

## 3. ANALYSIS OF THE INTERACTION BETWEEN BURSIAN AND DIOCOTRON INSTABILITIES

If  $I_0 > i(t) > I_{cr}$  (where  $I_0$  is the maximum current,  $i(t)$  is the instantaneous current value, and  $I_{cr}$  is the critical current), then Bursian instability begins to develop in the system and a nonstationary VC forms, which is usually characterized by a complicated spatiotemporal dynamics [20, 21, 29, 50–52, 54–59]. Simultaneously, the strong magnetic self-field of the

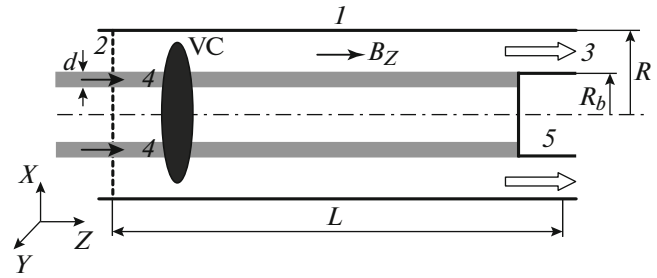


**Fig. 1.** Scheme of the model: (1) cylindrical drift chamber, (2) REB injection plane, (3) coaxial waveguide port, (4) monovelocity annular REB, and (5) cylindrical collector.

REB creates conditions for the onset of diocotron instability even in the absence of an external magnetic field [45].

We have thoroughly analyzed specific features of VC formation within the above relativistic vircator model. It is found that, before VC formation, the configuration of the high-order eigenmode excited in the system is such that it causes azimuthal rotation of the beam. In this case, one part of the electron beam rotates clockwise over the azimuth, while the other rotates counterclockwise [45]. As a result, in the azimuthal region where the electron flows move towards one another, the initial perturbation of the space charge density increases. This, in turn, leads to the onset of diocotron instability and the subsequent filamentation of the beam.

It is worth noting that the formation of a VC in the REB favors the onset of diocotron instability due to the accumulation of the space charge in the VC region, which leads to a substantial increase in the initial azimuthal perturbation of the space charge density in and, as a consequence, to the formation of a pronounced electron bunch in a certain azimuthal region in the plane perpendicular to the REB propagation direction (the  $XY$  plane).

Due to the formation of the electron bunch (structure) in the azimuthal direction, the beam is reflected back to the injection plane nonuniformly over the azimuth, most electrons being reflected from the region with the increased space charge density, i.e., from the region of the formed bunch, where the local decrease in the potential is maximum. We note that, simultaneously with the appearance of the first reflection, the electron structure and the region of electron reflection begin to rotate in the azimuthal direction due to the presence of the longitudinal magnetic field. As the beam current  $i(t)$  increases further, the bunch charge grows and, at a certain critical value at which the focusing forces can no longer compensate for the increased Coulomb repulsion forces, the bunch is divided into two bunches, thereby reducing the charge accumulated in each bunch. This makes the new REB

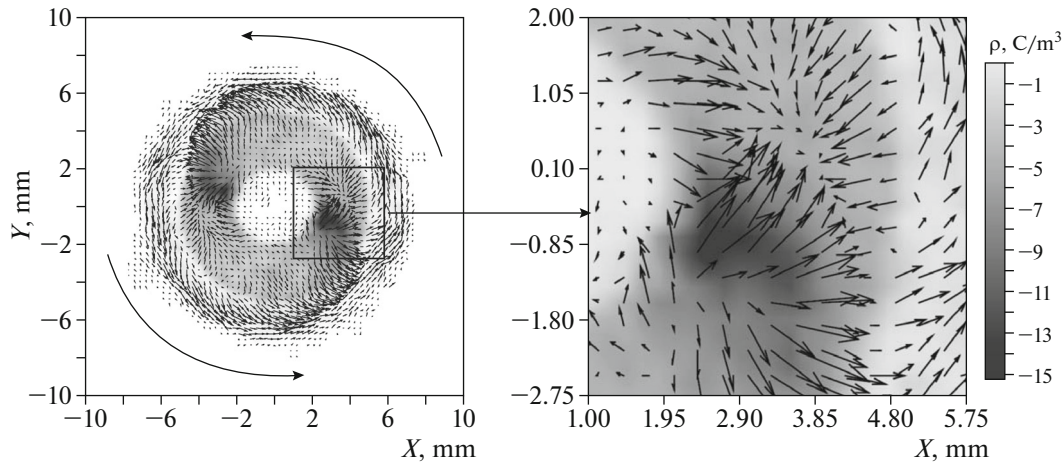


**Fig. 2.** Distribution of the space charge density in the  $XY$  plane superimposed with the vector field of electron beam velocities. The inset shows the enlarged fragment of the bunch region. The external magnetic field is  $B_0 = 1.85$  T, and the beam wall thickness is  $d = 3$  mm.

configuration stable in the azimuthal direction. If the current continues to grow, the formed structure becomes unstable again and the new separation of bunches occurs.

Let us examine the REB dynamics in the VC region in more detail. Figure 2 shows the distribution of the space charge density in the  $XY$  plane, superimposed with the vector field of electron flow velocities. The shades of gray show the value of the space charge density: the darker regions correspond to the higher space charge density. The arrows show the rotation directions of electron bunches. It is seen from Fig. 2 that, for the given parameters of the system, two electron bunches form in the azimuthal direction. The electron motion in the bunch region (see the enlarged fragment on the right of Fig. 2) is such that, on one side (on the bottom of the fragment), the electrons recede and the space charge density decreases, whereas on the other side, the electrons move toward one another and the space charge density increases. As a result, the bunches begin to rotate in the azimuthal direction.

We have paid special attention to the effect of the beam wall thickness  $d$  and the external magnetic field  $B_0$  on the simultaneous development and interaction of Bursian and diocotron instabilities. The beam wall thickness  $d$  was varied from 0.4 to 4 mm, while the external magnetic field  $B_0$  was varied from 0 to 2 T. It is found that, in this parameter range, from two to nine electron bunches rotating in the azimuthal direction can form in the beam. To illustrate typical regimes of the REB dynamics with developed Bursian and diocotron instabilities, Fig. 3 shows the distributions of the space charge density in the VC region in the  $XY$  plane and the corresponding beam configuration portraits, demonstrating the distributions of the electron energy. We note that each bunch periodically dumps

its charge, due to which electron filaments stretched along the beam axis form in the system. In the course of the further beam propagation and rotation the drift space, these filaments transform into a characteristic helical structure.

To more thoroughly analyze the processes occurring in the REB during the simultaneous development of Bursian and diocotron instabilities, we divided the  $(d, B_0)$  plane (beam wall thickness vs. external magnetic field) into regions corresponding to different numbers of electron bunches formed in the REB (see Fig. 4). It is seen from Fig. 4 that, at certain values of the beam wall thickness, the REB dynamics changes abruptly, namely, as  $d$  decreases, the number of the formed electron bunches increases from two to nine via a sequence of stepwise transformations of dynamic regimes. We note that the smaller the beam wall thickness  $d$ , the lesser variation in  $d$  is required for switching between the regimes. It is also seen that the effect of the external magnetic field is more complicated and its variation can lead to an increase or a decrease in the number of electron structures formed in the REB.

To better understand how the physical processes occurring in the REB depend on the parameters  $d$  and  $B_0$ , let us consider a simplified model that qualitatively describes the dynamics of the system. We represent electron bunches as point charges with the same charge  $-q$  ( $q > 0$  is the absolute value of the charge) arranged uniformly along the azimuth and rotating with the frequency  $\omega$  over a circle of radius  $R_m = R_b - d/2$  around the axis of the drift space. Then, in the laboratory frame, each charge experiences the centripetal acceleration  $a = R_m \omega^2$  under the action of the Lorentz force  $F_L = q(N)R_m \omega B_0$  and is

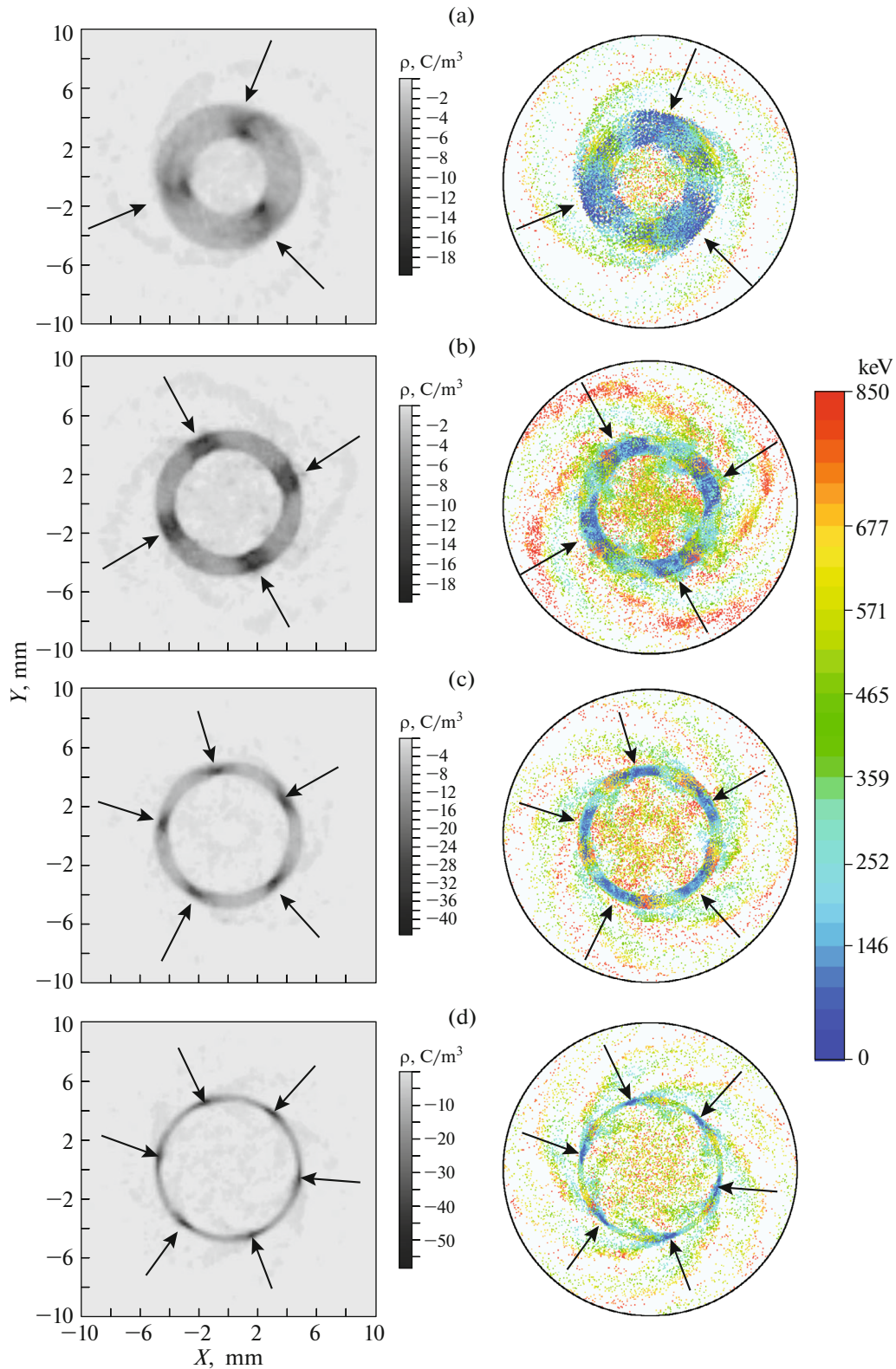


**Fig. 3.** (Color online) Distributions of the space charge density in the  $XY$  plane in the VC region and the corresponding configuration portraits of the beam for modes with different numbers  $N$  of electron bunches: (a)  $N = 3$  (at  $B_0 = 0$  T and  $d = 2.5$  mm), (b)  $N = 4$  ( $B_0 = 0$  T,  $d = 1.5$  mm), (c)  $N = 5$  ( $B_0 = 0$  T,  $d = 1$  mm), and (d)  $N = 6$  ( $B_0 = 0$  T,  $d = 0.5$  mm).

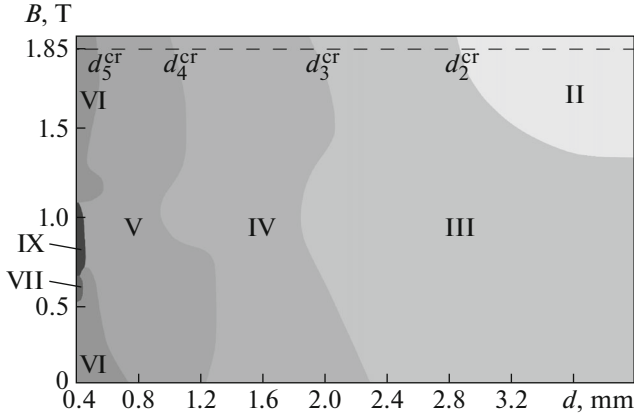


**Fig. 4.** Characteristic regimes of REB dynamics in the  $(d, B_0)$  plane (beam wall thickness vs. external magnetic field). Regions with different numbers  $N$  of electron bunches are shown with shades of gray. The Roman numbers denote the number of electron bunches in the azimuthal direction. The dependence in Fig. 5 is plotted for parameters corresponding to the dashed line. Here,  $d_2^{\text{cr}}$ ,  $d_3^{\text{cr}}$ ,  $d_4^{\text{cr}}$ , and  $d_5^{\text{cr}}$  are the critical values of the beam wall thickness for regimes with  $N = 2-5$ .

subject to the Coulomb repulsion force  $F_C = q(N)E_r(N)$ , where

$$E_r(N) = \frac{q(N)k}{R_m^2} \times \left( \sum_{i=1}^{\lfloor (N-1)/2 \rfloor} \frac{\cos \frac{\pi(N-2i)}{2N}}{\left(1 - \cos \frac{2\pi i}{N}\right)} + \frac{\delta(N \bmod 2)}{4} \right), \quad (1)$$

is the electric field created by the other charges. Here,  $N$  is the number of electron bunches,  $k$  is the proportionality coefficient (in SI units), and  $\delta$  is the delta function.

Thus, we obtain the equation

$$q(N)R_m\omega B_0 - q(N)E_r(N) = mR_m\omega^2, \quad (2)$$

where  $m$  is the mass of the point charge.

Using Eqs. (1) and (2), we find the equilibrium charge  $q_{\text{eq}}$  of an individual bunch at which the system of point charges rotates uniformly,

$$q_{\text{eq}}(N, d) = \frac{(R_b - d/2)^3 \omega}{E_r'(N)} \left( B_0 - \frac{\omega}{\eta} \right), \quad (3)$$

where  $E_r'(N) = E_r(N)(R_b - d/2)^2/q(N)$ .

Let us now consider how  $q_{\text{eq}}(N, d)$  varies with decreasing beam wall thickness  $d$  at fixed values of  $\omega$  and  $B_0 = 1.85$  T. On one hand, it is seen from expression (3) that a decrease in  $d$  leads to an increase in the equilibrium charge; on the other hand, it follows from

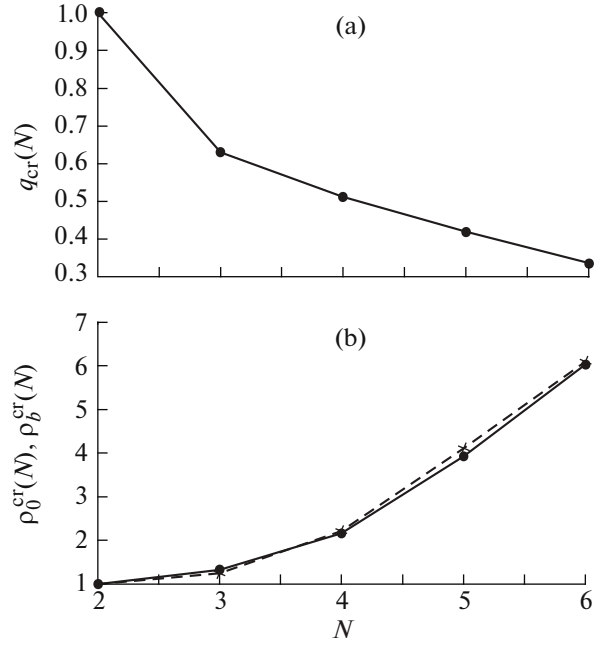


**Fig. 5.** (a) Critical value of the bunch charge  $q_{\text{cr}}(N)$  normalized to  $q_{\text{cr}}(N=2)$  as a function of the number of bunches  $N$ . (b) Critical value of the unperturbed space charge density  $\rho_0^{\text{cr}}(N)$  normalized to  $\rho_0^{\text{cr}}(N=2)$  (solid line) and critical value of the space charge density in the bunch  $\rho_b^{\text{cr}}(N)$  normalized to  $\rho_b^{\text{cr}}(N=2)$  (dashed line) as functions of the number of electron bunches  $N$ . The external magnetic field in both panels is  $B_0 = 1.85$  T.

Fig. 4 that, at a certain critical value  $d_N^{\text{cr}}$ , the number of electron bunches  $N$  increases and, as a result (see expression (3)),  $E_r'(N)$  increases, while  $q_{\text{eq}}(N, d)$  decreases. We introduce the critical (maximum) charge  $q_{\text{cr}}(N)$  for each regime and consider how its ratio to the critical charge at  $N = 2$  varies when switching between regimes with different  $N$ ,

$$\frac{q_{\text{cr}}(N)}{q_{\text{cr}}(N=2)} = \frac{(R_b - d_N^{\text{cr}}/2)^3 E_r'(N=2)}{E_r'(N)(R_b - d_{N=2}^{\text{cr}}/2)^3}. \quad (4)$$

Ratio (4) as a function of  $N$  is shown in Fig. 5a.

When plotting this dependence, the critical beam wall thickness  $d_N^{\text{cr}}$  was taken from numerical simulations (see Fig. 4). The ratio  $q_{\text{cr}}(N)/q_{\text{cr}}(N=2)$  shows how much the value of the critical equilibrium charge varies when switching from the regime with  $N = 2$  to a regime with  $N$  bunches due to a decrease in  $d$ . It follows from Fig. 5a that the critical charge  $q_{\text{cr}}(N)$  decreases monotonically with increasing number of bunches  $N$ . Thus, a change in the number of electron bunches  $N$  more strongly affects the value of the equi-

librium charge than a change in the beam wall thickness  $d$ .

We note that, as the beam wall thickness decreases, the space charge density in the unperturbed REB (i.e., its density at the point of injection into the system  $\rho_0(d) = I_0/(\pi(2R_b d - d^2)v)$ , where  $v$  is the initial beam velocity and  $I_0$  is the injection current) increases, which, in turn, leads to an increase in the average space charge density in the VC region and, consequently, in the space charge density in the bunches themselves ( $\rho_b(d)$ ), because  $\rho_0(d) \sim \rho_b(d)$ . By analogy with the earlier introduced critical charge  $q_{cr}(N, d_N^{cr})$ , we introduce the critical space charge density of the unperturbed REB for each regime,  $\rho_0^{cr}(N) = \rho_0^{cr}(d_N^{cr})$  (the maximum space charge density of the injected REB for the regime with  $N$  bunches), and the critical space charge density in the bunches themselves,  $\rho_b^{cr}(N) = \rho_b^{cr}(d_N^{cr})$ . Let us consider how these critical densities vary when switching between the regimes. To this end, we normalize the densities  $\rho_0^{cr}(d_N^{cr})$  and  $\rho_b^{cr}(d_N^{cr})$  to  $\rho_0^{cr}(d_2^{cr})$  and  $\rho_b^{cr}(d_2^{cr})$ , respectively. Thus, the change in the critical value of the space charge density of the unperturbed REB is determined by the expression

$$\frac{\rho_0^{cr}(d_N^{cr})}{\rho_0^{cr}(d_2^{cr})} = \frac{d_2^{cr}(2R_b - d_2^{cr})}{d_N^{cr}(2R_b - d_N^{cr})}, \quad (5)$$

where the critical value of the beam wall thickness  $d_N^{cr}$  is found from numerical simulations. For the change in the critical space charge density of the bunches, we have

$$\frac{\rho_b^{cr}(d_N^{cr})}{\rho_b^{cr}(d_2^{cr})} = \frac{q_{cr}(N, d_N^{cr})V_b(N=2, d_2^{cr})}{V_b(N, d_N^{cr})q_{cr}(N=2, d_2^{cr})}. \quad (6)$$

Here,  $V_b$  is the bunch volume, which is proportional to the beam wall thickness  $d$  and the bunch length in the azimuthal direction  $R_m \delta\phi$ , where  $\delta\phi$  is the angular size of the bunch. The angular size of the bunch is inversely proportional to the number of bunches  $N$  ( $\delta\phi \sim 1/N$ ), because they are distributed uniformly over the azimuth. This, for the bunch volume, we obtain

$$V_b \sim \frac{d_N^{cr}(R_b - d_N^{cr}/2)}{N}. \quad (7)$$

Using expressions (3), (6), and (7), we obtain the following expression for the critical space charge density in the bunches:

$$\frac{\rho_b^{cr}(d_N^{cr})}{\rho_b^{cr}(d_2^{cr})} \sim \frac{(R_b - 1/d_N^{cr})^2 d_2^{cr} N E_r'(2)}{(R_b - 1/d_2^{cr})^2 d_N^{cr} 2 E_r'(N)}. \quad (8)$$

Figure 5b shows how the critical space charge density in the unperturbed REB (solid line) and the critical

space charge density in the bunches (dashed line) depend on the number  $N$  of bunches (from 2 to 6). When plotting these dependences, the critical beam wall thickness  $d_N^{cr}$  was taken from numerical simulations (see Fig. 4,  $B_0 = 1.85$  T). It is seen that both critical space charge densities increase with increasing number of bunches  $N$ . At  $N > 4$ , the dependences are close to linear. We note that both dependences almost coincide, which confirms the correctness of our model.

Summarizing the aforesaid, we may conclude that, as the beam wall thickness  $d$  decreases, the space charge density in the VC region increases and, at a certain critical value at which the repulsion forces become higher than the focusing forces, the balance of forces is violated, the bunches split up, and the charge is redistributed among the large number of bunches. As the number of bunches increases, the average charge of the bunch decreases and the balance of forces is restored. The fragmentation of bunches and the decrease in the charge of each bunch make the new configuration stable, which agrees with the model described above.

Let us now consider how the increase in the magnetic field affects the processes occurring in the REB. On one hand, an increase in the magnetic field results in the compression (focusing) of the beam, which leads to an increase in the space adopted model, the focusing Lorentz force confining the bunches also increases with increasing magnetic field. The space charge density in the bunches depends nonlinearly on the external magnetic field (the space charge density increases rapidly at low magnetic fields and saturates at strong magnetic fields), while the Lorentz force within our model increases linearly with increasing  $B_0$  (see Eq. (2)). It is also worth noting that the form of the dependence  $\rho(B_0)$  differs for different  $d$  and the space charge density increases faster with increasing magnetic field at smaller  $d$ . The complicated behavior of regimes with different numbers of bunches under variations in the external magnetic field can be explained by the competition of the above processes.

Thus, for  $d$  in the range of 0.4–0.5 mm, the number of electron bunches first increases with increasing magnetic field and, then, decreases (see Fig. 4). This can be explained as follows. As the external magnetic field increases, the Coulomb repulsion forces between bunches grow due to the increase in their charges faster than the Lorentz force confining the electron bunches rises. At a certain critical value of the magnetic field, the Coulomb forces increase so much that they cannot longer be balanced by the focusing Lorentz forces. Then, the number of bunches increases and the charge is redistributed among them, due to which the average charge of the bunch decreases and the new configuration becomes stable. As the magnetic field increases further, the Coulomb

forces increases more slowly due to a decrease in the derivative of the function  $\rho(B)$ , while the Lorentz force continues to grow linearly. As a result, at a certain value of the magnetic field, the Lorentz forces become stronger than the Coulomb forces for the given REB configuration. In this case, fragmentation of bunches caused by the development of instabilities terminates earlier than at lower values of the external magnetic field, because the force balance is satisfied at a lower number of bunches, which agrees with the map of regimes in Fig. 4.

At large  $d$  ( $d > 2.8$  mm), the number of electron bunches decreases with increasing external magnetic field, because the balance of forces in this case is reached at a lower number of bunches. It is worth noting the following feature: at  $d > 3.5$  mm, the magnetic field at which the number of bunches begins to decrease coincides with the magnetic field at which the equilibrium radius of the electron beam  $R_{\text{eq}}$  becomes equal to the radius of the drift tube  $R$ . The magnetic field at which  $R_{\text{eq}} = R$  can be found by analyzing electron motion with allowance for the balance of forces [52],

$$B(R_{\text{eq}}) = R_{\text{eq}} \sqrt{\frac{\sqrt{2} I_0 \gamma_0^{3/2}}{\pi \epsilon_0 \eta^{3/2} \sqrt{V_0} (R_{\text{eq}}^4 - R_b^4)}}, \quad (9)$$

where  $V_0$  is the accelerating voltage,  $\eta$  is the specific electron charge,  $\gamma_0$  is the relativistic factor of the injected beam.

Setting  $R_{\text{eq}} = 10$  mm in expression (9), we obtain  $B(R_{\text{eq}} = R) \approx 1.31$  T, which agrees well with the map of regimes in Fig. 4.

We note that, at the boundary between the regimes, the system demonstrates a hysteresis: depending on the initial conditions, regimes with different numbers of electron bunches corresponding to one of neighboring domains in the map of regimes can be established due to the development of instabilities (see [60] for details).

#### 4. CONCLUSIONS

The dynamics of an annular REB with a VC has been studied numerically by using the CST Particle Studio software package. It is found that, in an annular REB with a supercritical current, Bursian and diocotron instabilities can develop simultaneously. The development of Bursian instability favors the development of diocotron instability due to the increase in the space charge density near the beam injection caused by the deceleration of the beam and the formation of a VC. Due to the interaction between instabilities, the VC acquires a complicated azimuthal structure consisting of electron bunches rotating in the azimuthal direction, which serve as reflection regions. The rotation of bunches results in the formation of a helical

electron structure stretched along the drift space. The effect of the beam wall thickness and the external magnetic field on the interaction between instabilities has also been analyzed. It is shown that a decrease in the beam wall thickness  $d$  leads to an increase in the number of electron bunches rotating in the azimuthal direction (in this work, regimes with the maximum number of bunches  $N = 9$  were observed) due to the increase in the space charge density. The effect of the external magnetic field is more complicated and can lead to an increase or a decrease in the number of bunches in the azimuthal direction.

#### ACKNOWLEDGMENTS

The study of the effect of the REB wall thickness on the dynamics of the system was supported by the Russian Science Foundation (project no. 14-12-00222). The study of the evolution of an REB with a VC under variation of the external magnetic field was supported by the Ministry of Education and Science of the Russian Federation (task no. 3.6723.2017/BCh) and the Russian Foundation for Basic Research (project no. 15-52-04018). The study of the physical processes in the system was supported by the Russian Federation Presidential Program for State Support of Young Russian Candidates of Sciences (grant no. MK-5426.2015.2).

#### REFERENCES

1. J. Benford, J. A. Swegle, and E. Schamiloglu, *High-Power Microwaves* (CRC Press, Boca Raton, 2007).
2. R. E. Collin, *Foundations for Microwave Engineering* (Wiley, Hoboken, NJ, 2001).
3. R. J. Barker and E. Schamiloglu, *High-Power Microwave Sources and Technologies* (IEEE Press, New York, 2001).
4. D. I. Trubetskov and A. E. Hramov, *Lectures on Microwave Electronics for Physicists* (Fizmatlit, Moscow, 2003, 2004), Vols. 1, 2 [in Russian].
5. R. J. Barker, J. H. Booske, N. C. Luhmann, and G. S. Nusinovich, *Modern Microwave and Millimeter-Wave Power Electronics* (Wiley, New York, 2005).
6. A. A. Koronovskii, D. I. Trubetskov, and A. E. Hramov, *Methods of Nonlinear Dynamics and Chaos in Problems of Microwave Electronics*, Vol. 2: *Nonstationary and Chaotic Processes* (Fizmatlit, Moscow, 2009) [in Russian].
7. A. M. Ignatov and V. P. Tarakanov, *Phys. Plasmas* **1**, 741 (1994).
8. H. S. Uhm, *J. Applied Phys.* **56**, 2041 (1984).
9. T. Klinger, C. Schroder, D. Block, F. Greiner, A. Piel, G. Bonhomme, and V. Naulin, *Phys. Plasmas* **8**, 1961 (2001).
10. Yu. P. Bliokh, G. S. Nusinovich, J. Felsteiner, and V. L. Granatstein, *Phys. Rev. E* **66**, 056503 (2002).
11. A. A. Koronovskii and A. E. Hramov, *Plasma Phys. Rep.* **28**, 666 (2002).

12. R. C. Davidson, *Theory of Nonneutral Plasmas* (Benjamin, New York, 1974).
13. R. B. Miller, *Introduction to the Physics of Intense Charged Particle Beams* (Plenum, New York, 1982; Mir, Moscow, 1984).
14. M. V. Nezlin, *Physics of Intense Beams in Plasmas* (Boca Raton, CRC Press, 1993).
15. R. C. Davidson, *Physics of Nonneutral Plasmas* (Imperial College Press/World Scientific, London, 2001).
16. R. C. Davidson and H. Qin, *Physics of Intense Charged Particle Beams in High Energy Accelerators* (World Scientific, Singapore, 2001).
17. M. V. Kuzelev and N. Sepekhri Javan, *Plasma Phys. Rep.* **33**, 672 (2007).
18. G. Shvets, O. Polomarov, V. Khudik, C. Siemon, and I. Kaganovich, *Phys. Plasmas* **16**, 056303 (2009).
19. V. R. Bursian and V. I. Pavlov, *Zh. Russ. Fiz.–Khim. Obshch.* **55**, 71 (1923).
20. L. S. Bogdankevich and A. A. Rukhadze, *Sov. Phys. Usp.* **14**, 163 (1971).
21. L. Thode, B. B. Godfrey, and W. R. Shanahan, *Phys. Fluids* **22**, 747 (1979).
22. V. I. Kuznetsov and A. Ya. Ender, *Plasma Phys. Rep.* **36**, 226 (2010).
23. V. I. Kuznetsov and A. Ya. Ender, *Plasma Phys. Rep.* **36**, 236 (2010).
24. R. A. Mahaffey, P. A. Sprangle, J. Golden, and C. A. Kapetanacos, *Phys. Rev. Lett.* **39**, 843 (1977).
25. A. N. Didenko, Ya. E. Krasik, S. F. Perelygin, and G. P. Fomenko, *Sov. Tech. Phys. Lett.* **5**, 128 (1979).
26. D. J. Sullivan, J. E. Walsh, and E. A. Coutsias, in *High-Power Microwave Sources (Artech House Microwave Library)*, Ed. by V. L. Granatstein and I. Alexeff (Artech House, Boston, 1987), p. 441.
27. A. E. Dubinov and V. D. Selemir, *J. Comm. Technol. Electron.* **47**, 575 (2002).
28. Yu. A. Kalinin and A. E. Hramov, *Tech. Phys.* **51**, 558 (2006).
29. A. S. Shlapakovski, T. Queller, Yu. P. Bliokh, and Ya. E. Krasik, *IEEE Trans. Plasma Sci.* **40**, 1607 (2012).
30. A. E. Dubinov, I. A. Efimova, K. E. Mikheev, V. D. Selemir, and V. P. Tarakanov, *Plasma Phys. Rep.* **30**, 496 (2004).
31. A. E. Hramov, A. A. Koronovsky, S. A. Kurkin, and I. S. Rempen, *Int. J. Electron.* **98**, 1549 (2011).
32. S. A. Kurkin, N. S. Frolov, A. O. Rak, A. A. Koronovskii, A. A. Kurayev, and A. E. Hramov, *Appl. Phys. Lett.* **106**, 1 (2015).
33. J. Ju, D. Cai, G. Du, Y. Wang, L. Liu, and J. Zhang, *IEEE Trans. Plasma Sci.* **43**, 3522 (2015).
34. A. L. Peratt and C. M. Snell, *Phys. Rev. Lett.* **54**, 1167 (1985).
35. C. C. Cutler, *J. Appl. Phys.* **27**, 1028 (1956).
36. R. L. Kyhl and H. R. Webster, *IRE Trans. Electron. Dev.* **3**, 172 (1956).
37. H. F. Webster, *J. Appl. Phys.* **28**, 1388 (1957).
38. I. N. Kartashov and M. V. Kuzelev, *Plasma Phys. Rep.* **36**, 524 (2010).
39. V. V. Mikhailenko, J. S. Kim, Y. H. Jo, V. S. Mikhailenko, and H. J. Lee, *Phys. Plasmas* **21**, 052105 (2014).
40. J. A. Rome and R. J. Briggs, *Phys. Fluids* **15**, 796 (1972).
41. C. A. Kapetanacos, D. A. Hammer, C. D. Striffler, and R. C. Davidson, *Phys. Rev. Lett.* **30**, 1303 (1973).
42. M. A. Mostrom and M. E. Jones, *Phys. Fluids* **26**, 1649 (1983).
43. Y. Carmel and J. A. Nation, *Phys. Rev. Lett.* **31**, 286 (1973).
44. V. V. Mikhailenko, H. J. Lee, V. S. Mikhailenko, and N. A. Azarenkov, *Phys. Plasmas* **20**, 042101 (2013).
45. S. A. Kurkin, A. A. Badarin, A. A. Koronovskii, and A. E. Hramov, *Phys. Plasmas* **22**, 122110 (2015).
46. C. K. Birdsall and A. B. Langdon, *Plasma Physics via Computer Simulation* (Taylor & Francis, New York, 2005).
47. S. A. Kurkin, A. A. Koronovskii, A. E. Hramov, and A. O. Rak, in *Proceedings of the 15th IEEE International Vacuum Electronics Conference, Monterey, CA, 2014*, p. 389.
48. M. Einat, M. Pilosof, R. Ben-Moshe, H. Hirshbein, and D. Borodin, *Phys. Rev. Lett.* **109**, 185101 (2012).
49. M. C. Balk, in *Proceedings of the 9th IEEE International Vacuum Electronics Conference, Monterey, CA, 2008*, p. 459.
50. S. A. Kurkin, A. E. Hramov, and A. A. Koronovskii, *Appl. Phys. Lett.* **103**, 043507 (2013).
51. S. A. Kurkin, A. A. Badarin, A. A. Koronovskii, and A. E. Hramov, *Phys. Plasmas* **21**, 093105 (2014).
52. A. E. Hramov, S. A. Kurkin, A. A. Koronovskii, and A. E. Filatova, *Phys. Plasmas* **19**, 112101 (2012).
53. S. E. Tsimring, *Electron Beams and Microwave Vacuum Electronics* (Wiley, Hoboken, NJ, 2007).
54. D. Biswas, *Phys. Plasmas* **16**, 063104 (2009).
55. R. A. Filatov, A. E. Hramov, Y. P. Bliokh, A. A. Koronovskii, and J. Felsteiner, *Phys. Plasmas* **16**, 033106 (2009).
56. G. Singh and S. Chaturvedi, *Phys. Plasmas* **18**, 063104 (2011).
57. S. A. Kurkin, A. A. Koronovskii, and A. E. Hramov, *Tech. Phys. Lett.* **37**, 356 (2011).
58. S. A. Kurkin, A. E. Hramov, and A. A. Koronovskii, *Tech. Phys. Lett.* **37**, 144 (2011).
59. N. S. Phrolov, A. A. Koronovskii, Yu. A. Kalinin, S. A. Kurkin, and A. E. Hramov, *Phys. Lett. A* **378**, 2423 (2014).
60. A. A. Badarin, S. A. Kurkin, and A. E. Hramov, *Bull. Russ. Acad. Sci., Physics* **79**, 1439 (2016).

*Translated by L. Mosina*